Specular and diffuse scattering of highly aligned phospholipid membranes

T. Salditt,[1] C. Münster,[1] J. Lu,[1] M. Vogel,[1,2] W. Fenzl,[2] and A. Souvorov[3]
[1]*Sektion Physik der Ludwig-Maximilians-Universität München, Geschwister-Scholl-Platz 1, D-80539 München, Germany*
[2]*Max-Planck Institut für Kolloid- und Grenzflächenforschung, Kantstrasse 55, D-14513 Teltow-Seehof, Germany*
[3]*European Synchrotron Radiation Facility, Boite Postale 220, F-38043 Grenoble Cedex, France*
(Received 15 June 1999)

We present a quantitative study of specular and diffuse (nonspecular) x-ray and neutron reflectivity from highly aligned phospholipid membranes deposited on solid substrates. The height-height correlation function could be obtained from the diffuse scattering without further model assumptions. The results differ significantly from the linear theory of smectic elasticity. We argue that the diffuse scattering is dominated by static liquid-crystalline defects, rather than thermal fluctuations. [S1063-651X(99)07312-2]

PACS number(s): 87.16.Dg, 61.10.Kw, 87.15.Ya

The statistical physics of phospholipid membranes has been studied for a long time. Apart from their significance as important model systems of biological membranes they represent interesting materials with a variety of unique properties. Phase transitions, elasticity, and fluctuation phenomena have all been studied both theoretically and experimentally [1]. By now, the concept of bending elasticity for multilamellar membranes in their fluid L_α state is well established [2]. Similarily, the molecular interactions responsible for a mean interlamellar distance d between membranes have been measured quantitatively, including electrostatic, van der Waals, hydration, and steric contributions [3,4]. It is now widely accepted, that multilamellar membrane fluctuations can be described by the linearized free energy density of a three-dimensional (3D) smectic liquid crystal

$$H/V=\frac{1}{2}B\left(\frac{\partial u}{\partial z}\right)^2+\frac{1}{2}K(\nabla_{xy}^2 u)^2, \tag{1}$$

where $u(x,y,z)$ is a continuum displacement field of the membranes with respect to a perfect lattice in the local coordinate system. $B[\mathrm{J/m^3}]$ and $K[\mathrm{J/m}]$ are the bulk moduli for compression and curvature, with K related to the bending modulus of a single membrane according to $K=K_s/d$.

With a few exceptions [5–7], the vast majority of experimental data on multilamellar membranes, in particular regarding the fluctuation analysis, have been collected on aqueous bulk suspensions. Due to the powderlike orientational distribution of domains, only limited information can be derived from such systems, e.g., in a scattering experiment. In this work we present a quantitative specular and diffuse reflectivity study of multilamellar phospholipid membranes deposited on a solid substrate, combining results from synchrotron x-ray and neutron experiments. We can determine the height-height correlation functions characterizing the multilamellar stack in a direct, and model independent way by recent advances in the analysis of high-resolution specular and diffuse scattering [8,9]. Apart from fundamental statistical physics, solid supported membrane systems are of interest for applications such as functionalized biomaterials. Furthermore, such studies are needed to shed more light on the one-dimensional crystallography of lipid-peptide or lipid-protein systems where detailed density reconstructions necessitate more rigorous approaches to fluctuation corrections of the raw data.

For our study we chose the well characterized phospholipid 1,2-dimyristoyl-sn-glycero-3-phosphatidylcholine (DMPC Avanti Lipids, AL). The samples were spread from isopropanol solution onto cleaned silicon substrates following a procedure given by Seul and Sammon [10]. After a slow evaporation process, the samples were put in a desiccator overnight to remove the organic solvent completly, and then rehydrated, resulting in a stack of mean thickness $D \simeq 13\,\mu$m. Finally, they were annealed in temperature cycles below and above the main chain transition to reduce lamellar defects. The orientational distribution (mosaicity) as measured in a rocking scan was typically smaller than the instrumental resolution (about 0.01°), see Fig. 1(a).

The resulting multilamellar stacks are put in a temperature and humidity controlled chamber (vapor phase at nearly 100 per cent relative humidity) for the x-ray investigation and were kept at a fixed temperature $T=45\,^\circ$C well above the chain melting transition to maintain the membranes in the liquid L_α state. The specular reflectivity was measured at an in-house rotating anode x-ray generator equipped with a Ge(110) channel cut monochromator selecting Cu$K_{\alpha 1}$ radiation and a NaJ scintillation counter. Extensive reciprocal space mappings of the diffuse scattering were carried out at the optics beamline of ESRF, Grenoble, using an unfocussed x-ray beam of 20 keV with a source divergence of about $1 \times 100\,\mu\mathrm{rad}^2$ (vertical x horizontal). Despite the highly brilliant synchrotron beam no radiation damage was observed even after exposure times of several hours which we attribute to the relatively low absorption cross sections at 20 keV. Complementing the x-ray data, we used diffuse neutron scattering in a scattering geometry, to obtain access to a wide range of reciprocal space [11]. The particular advantages of neutrons derive from the nearly perfect transperancy of the substrate to the neutron beam. This setup is ideally suited to map out the diffuse structure factor in the plane of incidence. In this geometry the resolution is intrinsically better than in a scan out of the plane of incidence, which must be used in the x-ray case [9,11]. The neutron experiments were carried out on the new ADAM reflectometer at the high flux reactor of ILL, Grenoble, under conditions described in Ref. [11].

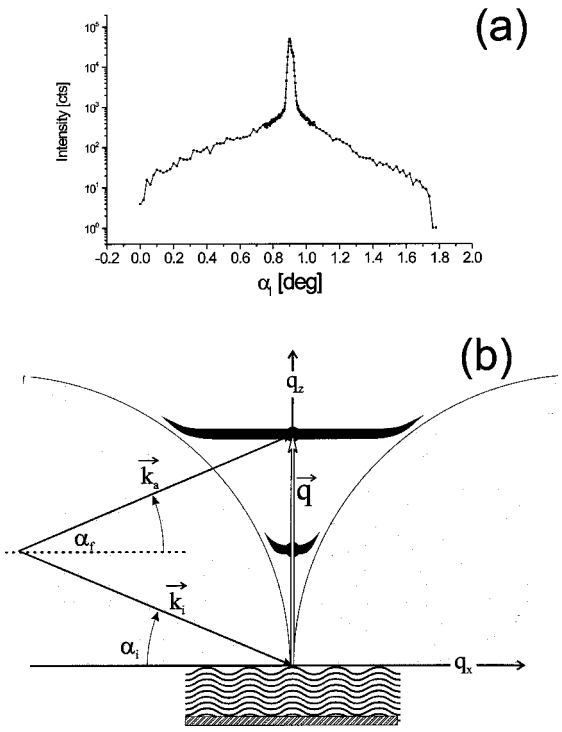

FIG. 1. (a) A representative rocking scan measured at the first Bragg peak, showing the sharp specular and the broad diffuse scattering component, respectively, in logarithmic representation. The perfect alignment is illustrated by a central width of about 0.014°. (b) A sketch of reciprocal space with the specular Bragg peaks on the q_z axis accompanied by the diffuse Bragg sheets extending into finite $q_\parallel$. The Bragg sheets can result from conformal thermal fluctulations or correlated layer distortions around lamellar defects. The form of a banana (or smile) is a result of refraction effects.

The x-ray reflectivity is displayed in Fig. 2(a) as a function of perpendicular momentum transfer q_z, as measured at $q_\parallel = 0$ $(q_{xy} = 0)$. $n = 7$ orders of multilamellar Bragg peaks are recorded, indicating a high degree of translational order and a well-defined lamellar periodicity of $d = 4.96$ nm. A density reconstruction was performed after phasing of the peaks yielding a membrane thickness of about $\delta_m = 3.7$ nm (headgroup-headgroup distance) and correspondingly a water layer of about $\delta_w = 1.3$ nm in between membranes. Despite a relative humidity in the chamber near 100 per cent, the bilayers were swollen only up to a repeat distance of about $d = 50$ Å, in agreement with a phenomenon known as the vapor pressure paradoxon [12]. The results were solidified by an independent reflectivity simulation (solid line) based on the Parratt algorithm using a box model for the bilayer density profile. The overall reflectivity decay and the existence of the higher order peaks is only reproduced well in the simulation if the rms value of bilayer fluctuations σ is kept below a value of $\sigma \simeq 0.3$ nm, in agreement with results found in bulk systems at equivalent osmotic pressures [13]. Within the harmonic model [17] the relationship $\sigma^2 = k_B T/(2\pi\sqrt{K_s B_s})$ can be derived. Taking, e.g., $\sigma = 0.2$ nm and a bending stiffness $K_s \simeq 0.8 \times 10^{-12}$ erg$(20 k_B T)$ for DMPC from the literature [13], a compressional modulus of about $B = 1.5 \times 10^8$ erg/cm^3 would be obtained.

However, as expected the simple Parratt model of perfect stacking and phase coherence with the substrate shows systematic descrepancies. In particular, the peak line shapes are not at all reproduced correctly in this model, as can be inspected by zooming the q_z range in (a). Contrarily, the alternative model based on truncation rod theory as discussed below, accounts quite well for the observed line shapes, see Fig. 2(b). Here, the normalized peaks of the different orders were plotted above each other against $q_z - q_c$, where q_c is the respective peak center. The line shapes of the different orders overlap perfectly except for the first order which is dynamically broadened by extinction owing to multiple (dynamic) reflections [14]. For $n \geqslant 2$, a half width at half maximum (HWHM) of 8.2×10^{-3} nm^{-1} indicates a domain size larger than $L \simeq 770$ nm. The solid line in (*d*) is a simulation according to

$$S(q_z) \propto \Big| \sum_{n=-N}^{n=N} \exp[-(nd/L)^2] \beta^{|n|} \exp[-n q_z d] \Big|^2, \quad (2)$$

with $N \ll L$ on the basis of a formula proposed in the context of crystal truncation rod scattering [15], where the first factor in the geometric sum takes into account the finite size L due to domain size or instrumental resolution, and $\beta = 0.98$ is an emperical line shape parameter, which will is given physical meaning further below. This form assumes (i) a perfect positional oder within one domain and (ii) a distribution of domains sizes which is incompatible with a single domain on the substrate or several coherent domains locked on the substrate in a fixed phase relationship [15].

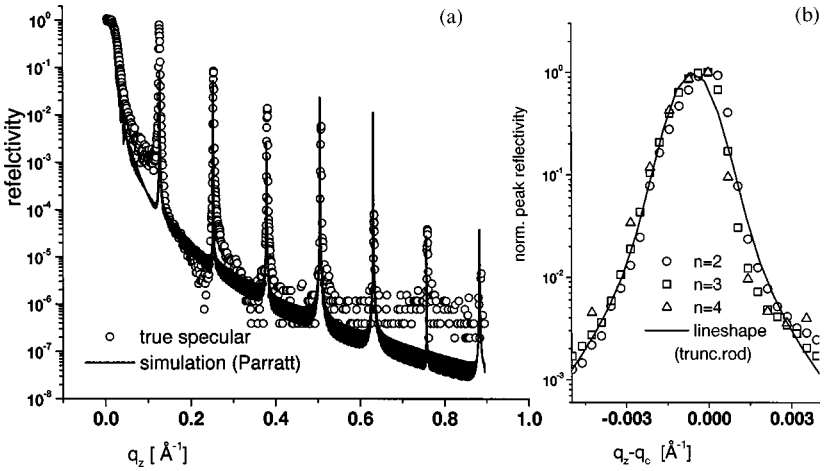

FIG. 2. (a) The reflectivity curve (open circles) of DMPC along with a simulation of a box model density profile of the stack calculated in the Parratt formalism (solid line). Systematic discrepancies in the peak line shapes are observed. (b) Normalized profiles of second, third, and fourth Bragg peak, scaling perfectly to a single lineshape fit (after subtracting the peak centers q_c), in contrast to the prediction of the Caillé model.

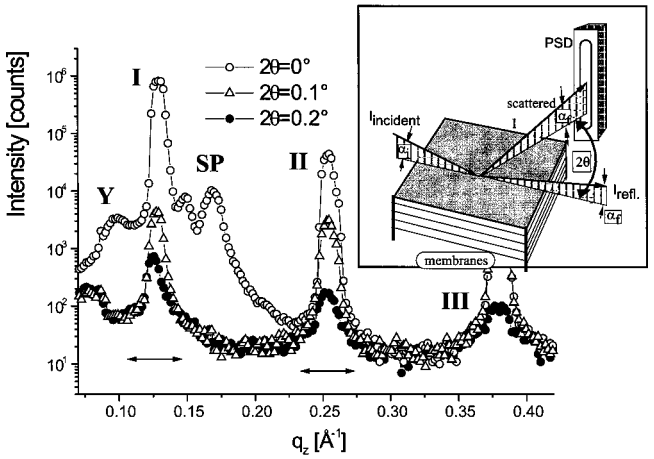

FIG. 3. X-ray diffuse scattering measured in the setup of grazing incidence diffraction (sketched in the inset): Three representative vertical slices through the diffuse Bragg sheets (orders n denoted by roman numbers) are shown as a function of q_z at different constant angles 2θ out of the plane of incidence. At $2\theta=0°$, the specular beam (SP) is observed in between the first and second order Bragg sheet.

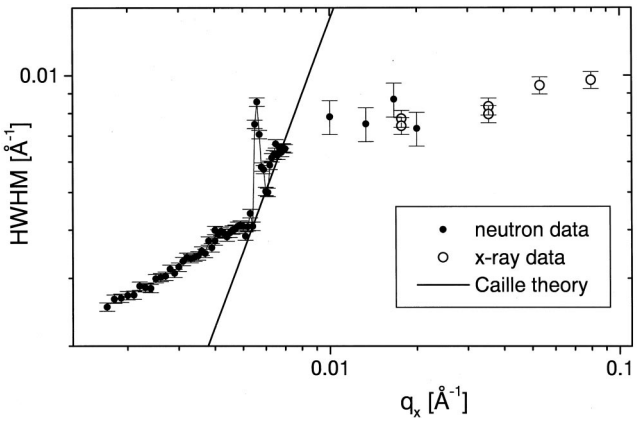

FIG. 4. The half width at half maximum (HWHM) in q_z of the first Bragg sheet as a function of $q_\parallel$, as obtained after combining neutron and x-ray data. The peak at 0.006 $Å^{-1}$ is due to a refraction effect (see text). For comparison, the quadratic scaling of the width according to the Caillé model is plotted as a solid line.

In particular, even before any data analysis, the lack of tail scattering clearly contradicts the usual algebraic decay in translational symmetry, well known as Landau-Peierls instability [4,16,17]: a logarithmic divergence of $\langle|u_i(r)-u_j(r')|\rangle$ as derived from Eq. (1) leads to an enhanced tail scattering described by a slope $2-\eta_n$ with $\eta_n = n_0 n^2$ [17]. Thus, the slope decreases strongly with the order n, which is not observed here. At the same time, the clear separation of specular and diffuse scattering indicates the absence of a logarithmic divergence also along the membranes in the xy plane, and hence a perfect long range positional order within the domains, both along the z and the lateral x,y directions. This is a surprising result, since the multilamellar stack is several thousands of bilayer thick, and the vast majority of membranes probed is far away from the substrate.

Let us now consider the nonspecular scattering contribution, arising from bilayer fluctuations or other types of lateral disorder. As is well known, the diffuse scattering of a multilayered system is a unique transformation of the statistical height-height difference functions (or correlation functions) defined as $g_{ij}(r)=\langle[u_i(r')-u_j(r'+r)]^2\rangle$, where u denotes the deviation from the mean average position of the interfaces labeled by i and j [8]. In particular, the average height-height self-correlation function ($i=j$) can be retrieved after a numerical back transformation of the structure factor $S(q_z,q_\parallel)$ [9], if the data has been collected over a wide enough range in $q_\parallel$, e.g., by scanning the reciprocal space both in and out of the plane of incidence. In Fig. 3 the diffuse intensity is shown as a function of q_z at different angles 2θ out of the plane of incidence, corresponding to increasing $q_\parallel$, from top to bottom scaled as measured. $\alpha_i=0.5°$ was kept constant throughout and chosen such that the specular peak (SP) was lying in between the first and second Bragg sheet to ensure that the diffuse sheets could be measured without excitation of the specular Bragg peak [9]. The scattering geometry of grazing incidence, in which such data can be measured, is shown in the inset, and has been described in detail before [9].

In Fig. 4 the half width at half maximum ω of the first Bragg sheet is plotted as a function of $q_\parallel$. For this purpose, results of x-ray diffuse scattering (measured in the setup shown in Fig. 3) and neutron diffuse scattering have been combined (technical aspects, in particular refraction effects like the peak at 0.0055 $Å^{-1}$ [18] are described in Ref. [11]). At small $q_\parallel$, the q_z width of the Bragg sheets is resolution dominated, while a broadening can be observed at intermediate values, before a saturation value is reached at high $q_\parallel$. The intrinsic q_z width ω of the Bragg sheet is inversely proportional to the correlation length ξ_z defined as the vertical decay length of fluctuations characterized by a lateral wave number $q_\parallel$,

$$g_{ij}(q_\parallel)\propto e^{-|i-j|d/\xi_z}. \tag{3}$$

According to the Caillé model, ξ_z should scale quadratically as

$$\xi_z=(\lambda q_\parallel^2)^{-1}, \quad \omega=\lambda q_\parallel^2. \tag{4}$$

The deviation of the data in Fig. 4 from this simple picture is obvious, even if resolution effects at small $q_\parallel$ are taken into account. The high $q_\parallel$ regime, on the other hand, may not be describable by a continuum theory, since the lateral length scales become too small. Therefore, one could argue, that only the intermediate regime, where the broadening is observed, should be considered to determine $\lambda := \sqrt{K/B}$, see the solid line. Remarkably, the corresponding value of $\lambda \simeq 14$ nm is more than an order of magnitude higher than the value of about 1 nm, which is be estimated from the above values of B and K. Apart from the mentioned discrepancy between data and theory, this result indicates that even in the intermediate regime the observed broadening is inconsistant with the fluctuation amplitude σ determined from the reflectivity.

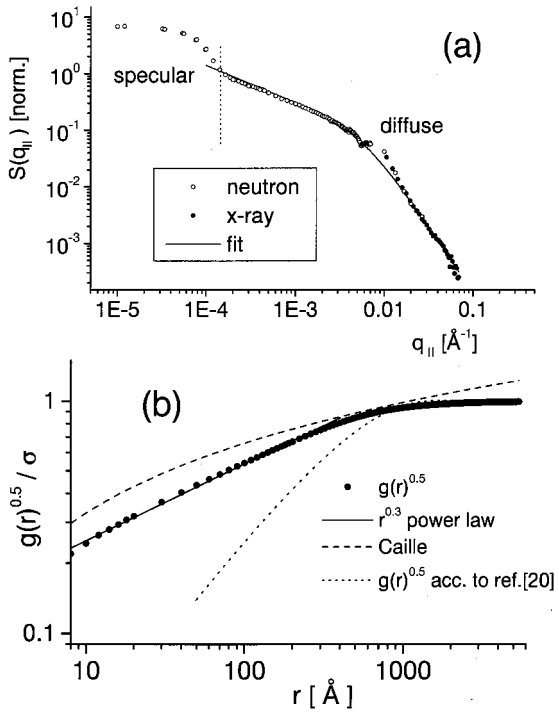

FIG. 5. (a) q_z-integrated intensities of the first diffuse Bragg sheet as a function of $q_\parallel$, combining neutron (open symbols) and x-ray (solid symbols) data. The overall profile is approximated by an analytical function (solid line) used to generate $g(r)$. The exponents found in the power-law regime are distinctly different from the Caillé theory. (b) Height-height difference function $g(r)^{0.5}$ as obtained by a numerical back transformation of the data in (a). For comparison the theoretic predictions of two different linear models are plotted (see text).

Let us now discuss the decay of the Bragg sheet intensity with 2θ or equivalently $q_\parallel$, which is quantified in Fig. 5(a). The intensity of the first and second Bragg sheet, respectively, is shown after integration along q_z over the corresponding width of the sheet, i.e., the width indicated by the horizontal arrows in Fig. 3. Again, the data points of the neutron experiments have been combined with those of the diffuse x-ray scattering measured out of the plane of incidence, and are found to agree well in the range of overlap [18].

In this representation of the q_z-integrated intensity, all contributions of the cross-correlation functions drop out and the structure factor $S(q_\parallel, q_{z,n}\,\text{const})$ corresponding to the average self-correlation function $g(r)$ is measured [19]. Below the specular peak a broad diffuse plateau with a small slope of about $q^{-0.65}$ is observed, followed by an asymptotic power law decay $q^{-2.56}$ for $q_\parallel \geqslant 0.006\,\text{Å}^{-1}$. The exponents associated with the asymptotic regime, $\gamma_1 = 2.56$ and $\gamma_2 = 2.14$ for the first and second Bragg sheet, respectively, differ drastically from the Caillé exponents. From the dependence of γ on the order of the Bragg sheet the fluctuation amplitude or rms roughness σ can be extracted along with the functional form of $g(r)^{0.5}$ by a numerical back transformation [9]. Since the details of the procedure in particular regarding the numerical treatments, the resolution, background and cutoff effects have been discussed before [9], only the results for $g(r)^{0.5}$ are presented in Fig. 5(b). For small r a power law of $g(r)^{0.5} \propto r^{0.3}$ is found, followed by a saturation regime at about $\xi_\parallel \simeq 100\,\text{nm}$. The functional form is compared with (i) the logarithmic function predicted by the Caillé model and (ii) to an analytical form given by Netz [20], valid in linear approximation for a single membrane near a hard wall or any harmonic pinning potential. Clearly, both models can be discarded.

Furthermore, it is important to note that the fluctuation amplitude $\sigma \simeq 14\,\text{Å}$ derived from the analysis of the diffuse intensity is much larger than that derived from the simulation of the specular reflectivity. Along with the discrepancies discussed above this may lead us to assume that the diffuse intensity at high $q_\parallel$ is dominated by inhomogeneous and localized static defects, leading to a highly conformal distortion of the layer lattice in the vicinity of the defects. This effect results in a higher effective amplitude determined from the diffuse scattering. Contrarily, the specular reflectivity is dominated by well ordered areas far away from defects, where mainly thermal fluctuations contribute to σ. In this picture, a single multilamellar domain breaks up into seperate phase-shifted domains by static lamellar defects [21], where the determined values for $\xi_\parallel$ would be a typical length scale of the distortion field associated with the defect, as observed also in some smectic liquid crystals [22]. The line shape parameter β used for the simulation in Fig. 2(b) may be linked to the defect probability. These conclusions are also supported by polarized optical microscopy observations: hydrated samples prepared by the same method on glass cover slides exhibit a texture of many isolated axissymmetrical focal conic defects.

In summary, we must put forward a picture of large and highly oriented, multilamellar domains, within which the bilayers are long-range ordered both in the lateral and normal directions. The suppression of the thermal fluctuations may possibly be due to the effective surface tension associated with the solid-lipid and the lipid-vapor interfaces, respectively [24]. The resulting absence of the Landau-Peierls instability has important consequences for one-dimensional crystallographic studies of lipids and lipid-protein systems, since the maximum resolution achievable under these conditions is no longer limited by thermal fluctuations as in the Caillé theory. The domains in turn are not in a positionally coherent, fixed phase relationship with each other, but are separated by defects, probably of focal conic type. The conformal layer distortions around the defects affect the diffuse scattering. Defect scattering has so far not been addressed in lipid membranes, but may have been a significant contribution also in many previous measurements of solid supported membranes and isotropical suspensions of bilayers with high bending rigidity [23]. Discrepancies between theory and inelastic neutron scattering experiments on partially hydrated films [25], where the relaxation times were found to be several orders of magnitude longer than expected, may also derive from the fact that the signal was affected by the defect dynamics rather than only thermal fluctuations. It should be noted, however, that the situation may be quite different in fully hydrated membranes, where thermal fluctuations are much more prominent.

In the future, the scaling of the defect scattering and the corresponding coefficients may be compared directly to theoretic expressions yielding details of elastic properties and

constants, including the coefficients of Gaussian curvature. A more complete understanding of these simple model systems of solid supported membranes will pave the way for quantitative analysis of more complex lipid-peptide and lipid-protein systems, where high orientational and positional order in conjunction with the present techniques can yield high spatial resolution in both the vertical and lateral dimension.

ACKNOWLEDGMENTS

We thank S. Moss, P. Davidson, C. Safinya, and R. Netz for fruitful discussions, and particularly J. Peisl and R. Lipowsky for their continous support. We are further grateful for the excellent beam and superb working conditions provided by the staff of ESRF.

[1] *Handbook of Biological Physics*, edited by R. Lipowsky and E. Sackmann (Elsevier, Amsterdam, 1955), Vol. 1.
[2] W. Helfrich, Z. Naturforsch. C **28**, 693 (1973).
[3] R. P. Rand and V. A. Parsegian, Biochim. Biophys. Acta **988**, 35 (1989), and references therein.
[4] C. R. Safinya, E. B. Sirota, D. Roux, and G. S. Smith, Phys. Rev. Lett. **62**, 1134 (1989); **57**, 2718 (1986).
[5] G. Smith, E. B. Sirota, C. R. Safinya, and N. A. Clark, Phys. Rev. Lett. **60**, 813 (1988).
[6] D. C. Wack and W. W. Webb, Phys. Rev. A **40**, 1627 (1989).
[7] M. Seul and P. Eisenberger, Phys. Rev. A **39**, 4230 (1989).
[8] S. K. Sinha, E. B. Sirota, S. Garoff, and H. B. Stanley, Phys. Rev. B **38**, 2297 (1988); S. K. Sinha, J. Phys. III **4**, 1543 (1994).
[9] T. Salditt, T. H. Metzger, and J. Peisl, Phys. Rev. Lett. **73**, 2228 (1994); Europhys. Lett. **32**, 331 (1995).
[10] M. Seul and M. J. Sammon, Thin Solid Films **185**, 287 (1990).
[11] C. Münster, T. Salditt, M. Vogel, R. Siebrecht, and J. Peisl, Europhys. Lett. **46**, 486 (1999).
[12] R. Podgornik and V. A. Parsegian, Biophys. J. **72**, 942 (1997).
[13] H. I. Petrache, *et al.*, Phys. Rev. E **57**, 7014 (1998).
[14] V. Holý *et al.*, Phys. Rev. B **47**, 15 896 (1993); V. Holý, T. Baumbach, *ibid.* **49**, 10 668 (1994).
[15] I. K. Robinson, Phys. Rev. B **33**, 3830 (1986).
[16] J. Als-Nielsen *et al.*, Phys. Rev. B **22**, 312 (1980).
[17] C. R. Cailleé, Acad. Sci. Ser. **274**, 891 (1972).
[18] The peculiar features in the neutron data at about $q_{\|} = 0.0055\ \text{Å}^{-1}$ stems from refraction effects occuring at the semicircles in Fig. 1 [11], i.e., upon crossing over from reflection to transmission geometry.
[19] T. Salditt *et al.*, Phys. Rev. B **51**, 5617 (1995); **54**, 5860 (1996).
[20] The linear equation discussed by Netz is obtained by replacing the first term in Eq. (1) by Bu^2, using an absolute rather than a relative displacement field, see R. Netz, Ph.D. thesis, University of Köln, 1994.
[21] S. A. Asher and P. S. Pershan, J. Phys. (France) **40**, 161 (1979).
[22] P. Davidson *et al.*, J. Phys. II **1**, 61 (1991).
[23] Note that the scattering experiments in Ref. [4] were carried out on lipid bilayers upon addition of pentanol, which considerably lowers the bending rigidity K_s, so that thermal fluctuations are dominating static defects, in contrast to the present study on membranes of much higher K_s.
[24] V. A. Parsegian and R. Podgornik, Colloids Surf., A **129**, 345 (1997).
[25] W. Pfeiffer *et al.*, Europhys. Lett. **23**, 457 (1993).